Article

Behavioral Model of G3-Powerline Communication Modems for EMI Analysis

Abduselam Hamid Beshir [1], Simone Negri [1], Xinglong Wu [1,*], Xiaokang Liu [1], Lu Wan [1,2], Giordano Spadacini [1], Sergio Amedeo Pignari [1] and Flavia Grassi [1]

[1] Department of Electronics, Information and Bioengineering (DEIB), Politecnico di Milano, 20133 Milan, Italy; abduselamhamid.beshir@polimi.it (A.H.B.); simone.negri@polimi.it (S.N.); xiaokang.liu@polimi.it (X.L.); lu.wan@polimi.it or luwa@energy.aau.dk (L.W.); giordano.spadacini@polimi.it (G.S.); sergio.pignari@polimi.it (S.A.P.); flavia.grassi@polimi.it (F.G.)

[2] Department of Energy, Aalborg University, 9220 Aalborg, Denmark

* Correspondence: xinglong.wu@polimi.it

Abstract: G3-powerline communication (G3-PLC) is a robust communication protocol originally developed for smart metering in low-voltage power distribution networks. Modeling G3-PLC modems is an essential task to investigate electromagnetic compatibility (EMC) issues related to the coexistence of the PLC signal with the high-frequency noise affecting low-voltage networks, mainly due to the presence of power converters and non-linear loads. Since detailed information on the modem internal architecture is usually not available to the end-user, this work investigates the possibility of developing behavioral (black-box) models of G3-PLC modems, whose parameters can be estimated starting from measurements carried out at the modem output ports. To this end, suitable test benches are set up and used for model-parameter extraction as well as for validation purposes. Experiments have proven that an equivalent representation involving non-ideal voltage sources (i.e., in terms of extended Thevenin/Norton equivalent circuits) is no longer feasible for the transmitting modem, since the presence of a closed-loop control system invalidates the linearity assumption. Hence, while the receiving modem is still modeled through an impedance matrix (since it behaves as a linear device), an alternative representation is proposed for the transmitting modem, which resorts to the use of two ideal voltage sources in accordance with the substitution theorem. Experimental results prove that the proposed modeling strategy leads to satisfactory predictions of the currents propagating on the PLC system in the frequency interval of interest. Hence, it could be used in combination with high-frequency models of the other components in the network to investigate EMC and the coexistence of the PLC signal with the high-frequency noise generated by power converters.

Keywords: conducted emission (CE); electromagnetic compatibility (EMC); electromagnetic interference (EMI); powerline communication (PLC)

1. Introduction

The integration of intermittent renewable energy sources and the penetration of active loads have made power system networks increasingly complex [1,2]. Additionally, the massive deployment of complex communication protocols makes electromagnetic interference (EMI) modeling even more challenging. Narrowband powerline communication (NB-PLC) technology, such as PRIME, G3-PLC, and IEEE 1901.2, is used in smart grid (SG) applications [3,4], offering the advantage of using existing power cables for both power and data transmission, thus minimizing cost and complexity [5–7]. An example of a PLC application is shown in Figure 1, where a PLC transmitter (PLC Tx) and receiver (PLC Rx) operate in a system integrating distributed generation (DG) sources, such as photovoltaics (PVs) and wind generators, with different, and possibly active, loads, such as smart buildings and electric vehicle chargers, which can behave as energy producers or consumers

depending on time. In this system, supra-harmonics in the frequency range from 2 to 150 kHz exiting power converters can be detrimental to the operation of NB-PLC systems, even if these systems usually employ robust modulation and error correction codes. Indeed, recent studies have evidenced coexistence issues between NB-PLCs and power converters, focusing on G3-PLC systems and randomly modulated power converters [8,9].
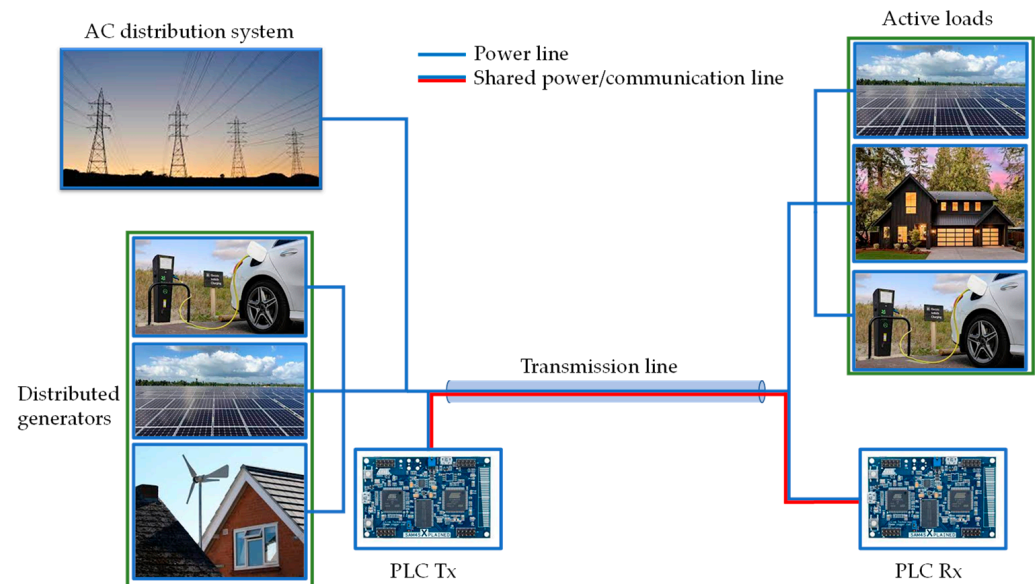

Figure 1. Schematic representation of a typical PLC application in modern distribution systems.

To investigate the coexistence issue between power converters and PLC communication systems in complex networks, such as SGs, it is important to develop accurate high-frequency models of both the power converters and the communication systems. To this end, there are two primary approaches available [10]. The first one, hereinafter referred to as "white-box", is based on a circuit representation of all individual components [11] and is often unpractical since it requires detailed information on the internal architecture of the device, including parasitics [12]. Additionally, integrating such PLC-system models into power system networks for EMI analysis is quite challenging due to the limited availability of suitable software tools. An alternative approach is the so-called "black-box" or behavioral modeling approach, which provides an equivalent representation of the device at its output ports. Model parameters are extracted from a suitable set of measurements without requiring any a-priori knowledge of the inner circuitry.

Due to these advantages, behavioral modeling of power converters for EMC analysis has received increasing attention. Examples are in [13,14], where the power converter is represented at the output ports in terms of an equivalent circuit with a minimum number of active and passive components (Thevenin/Norton equivalent circuits), whose frequency response is extracted from measurements. Although such an approach offers several advantages, it inherently assumes that the system is linear and time-invariant (LTI) [15]. This limitation is not necessarily affecting the modeling of power converters since they are usually equipped with large input capacitors and inductors, which mask the nonlinear behavior of the converter semiconductor devices [16,17]. Additionally, power converter control algorithms are designed to track low-frequency signals (DC or AC 50/60 Hz), so they are typically effective up to a few kHz at most. Hence, for EMI analyses, the noise generated by the power converter is marginally affected by the control algorithms, thus allowing for a circuit representation of the device in terms of the linear noise source. On the contrary, the linearity assumption may put a constraint on modeling PLC modems since the control loop of these devices is designed to inject controlled signals into the grid with a frequency up to some hundreds of kHz.

Despite recent research advancements, there is a research gap in finding accurate EMI models of PLC systems. While some studies [18,19] have proposed "white-box" circuit models of PLC modems aimed at investigating different PLC modulations, these models are too approximate to be used for EMI analysis in complex systems, such as SGs. There are also some interesting studies on the channel characterization of PLC systems for various applications [20,21]. Some modal-based modeling and analysis methods have been proposed as well [22,23]. However, coexistence issues between power converters and PLC systems are still under investigation [24].

Therefore, this work aims at providing a behavioral representation of the G3-PLC system, which can be easily integrated into complex power networks with the objective of predicting coexistence issues with the powerline noise. To this end, it is first investigated whether G3-PLC modems can be modeled as linear non-ideal sources. To this end, the transmitting G3-PLC modem (PLC Tx) is modeled by an extended Thevenin equivalent circuit, while the receiving PLC modem (PLC Rx) is represented by an impedance matrix. A set of experiments, however, will reveal that when the modem is in transmit mode, the linearity assumption is no longer satisfied due to the presence of closed-loop control algorithms. Hence, in accordance with the substitution theorem, an alternative representation involving a pair of ideal voltage sources is proposed for the transmitting modem, which led to appreciable agreement with measurement data under different operating conditions.

The remaining part of the manuscript is organized as follows: the system under analysis is introduced and described in Section 2. Section 3 discusses the details of employing standard Thevenin/Norton modeling procedures in PLC applications. The experimental investigation of this first behavioral model is presented in Section 4. An alternative model and its experimental validation are provided in Section 5. Final conclusions are drawn in Section 6.

2. System under Analysis

In order to investigate the issues related to PLC operation in noisy environments and to predict EMI in complex systems, detailed models of each unit of the system are required. This work focuses on PLC modeling, and therefore a simplified setup, shown in Figure 2, is considered. The simplified setup is aimed at representing a basic radial distribution network, where the system under analysis is supplied by the AC mains (230 V, single phase) through a short cable, and two PLC modems are connected to the power line. Additionally, two Line Impedance Stabilization Networks (LISNs) are included in the setup with the following three purposes: Firstly, LISNs reject high-frequency noise possibly coming from the AC mains and provide a stable impedance in the frequency range of interest. This allows for the removal of possible sources of uncertainty, which is beneficial for the PLC model's accuracy. Secondly, they provide additional measurement ports for measuring EMI. Finally, different LISNs can be used to offer a different set of impedances in the frequency range of interest for PLC modeling without affecting the low-frequency system behavior, allowing for multiple tests in well-defined conditions that provide the data needed to verify the proposed behavioral model. The oscilloscope is connected to the measurement ports of the two LISNs in order to simultaneously measure the EMI coming from the system under analysis. It is worth noting that the schematic shown in Figure 2 is used not only for behavioral modeling but also for validation measurement. Specifically, in the validation stage, the circuit layouts of the LISNs are different from the ones used for model extraction, providing data from different system working conditions.
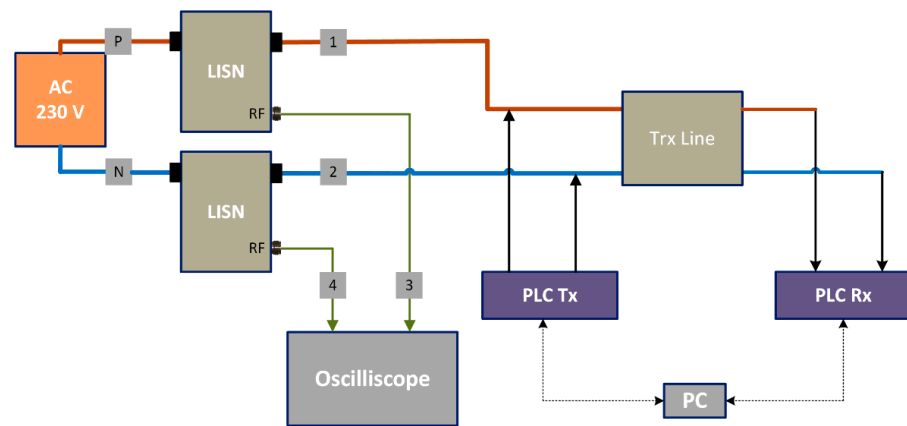
Figure 2. Principal diagram of the setup for PLC modeling.

3. Behavioral Modeling Procedure

In this section, the procedure used to derive a Thevenin equivalent model representing the considered PLC system is presented. Norton equivalent circuits are not discussed for brevity, as they are a dual (equivalent) representation of the Thevenin model discussed in the following. The procedure to extract the passive part of the Thevenin model and to characterize the other passive elements of the system depicted in Figure 2 is described in Section 3.1. The procedure to extract the active part of the PLC Thevenin model is presented in Section 3.2.

3.1. Characterization of Passive Elements

The circuit reported in Figure 2 can be subdivided into three main blocks: (1) PLC Tx; (2) transmission line and PLC Rx; and (3) AC mains and LISNs. Each of these elements is characterized by vector network analyzer (VNA) measurements in terms of S-parameters. The following subsections present the procedure to determine the equivalent circuit representation of the passive part of those elements.

3.1.1. Characterization of the PLC Tx and Rx Modems

Since one of the PLC modems is operated as a transmitter (PLC Tx) and the other one is operated as a receiver (PLC Rx), it is reasonable to use an extended Thevenin equivalent circuit for the PLC Tx unit, while the PLC Rx unit is modeled simply by an impedance matrix, i.e., the passive part of the Thevenin model. The Thevenin equivalent circuit for a two-port circuit element, used in the following for the PLC Tx, is shown in Figure 3a, while the equivalent passive model, used in the following for the PLC Rx, is depicted in Figure 3b.
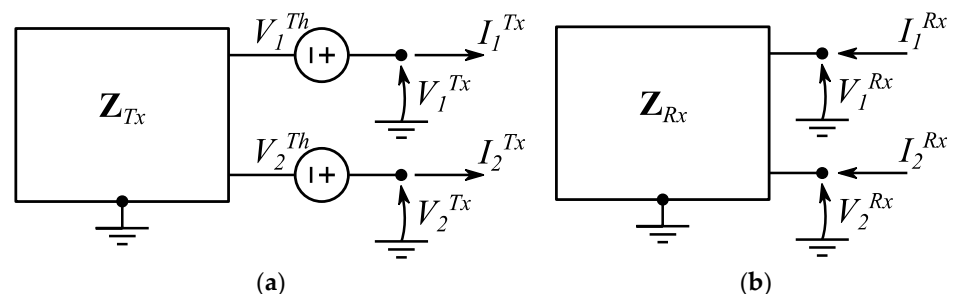

(**a**)   (**b**)

Figure 3. Behavioral model representation of PLC modems: (**a**) Thevenin equivalent circuit for the PLC Tx, and (**b**) impedance representation for the PLC Rx.

The PLC Tx and Rx modems are characterized independently by means of a VNA measurement. The PLC Tx is characterized as a two-port network, as shown in Figure 4a, when it is switched off. The measurement results in a 2 × 2 S-parameters matrix, denoted

hereon as $\mathbf{S}_{Tx}$, from which the passive part of the Thevenin model is extracted. The transmission line (Trx Line) should also be characterized and then cascaded with the S-parameter matrix of PLC Rx. To account for the effects of the transmission line interconnecting the two modems (whose modeling is beyond the scope of this analysis), this stretch of cable is directly characterized together with the PLC Rx, as shown in Figure 4b. The measurement results in a 2 × 2 S-parameter matrix, denoted hereon as $\mathbf{S}_{Rx}$, which includes the effects of the cable interconnecting the two modems in addition to those due to the modem itself.
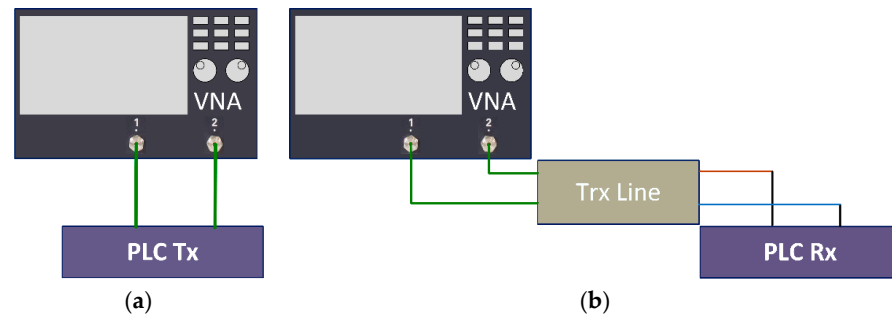

(a)   (b)

Figure 4. Characterization of (**a**) PLC Tx and (**b**) PLC Rx and transmission line.

The corresponding impedance matrices $\mathbf{Z}_{Rx}$ and $\mathbf{Z}_{Tx}$ are obtained as follows:

$$\mathbf{Z}_{Rx,Tx} = Z_0(\mathbf{I}_2 + \mathbf{S}_{Rx,Tx})(\mathbf{I}_2 - \mathbf{S}_{Rx,Tx})^{-1} \tag{1}$$

where Z_0 is the reference impedance, in this case equal to 50 Ω, and $\mathbf{I}_2$ is the 2 × 2 identity matrix.

3.1.2. Characterization of the LISNs

The considered setup includes two identical LISNs connected to the phase and neutral wires of the AC mains. In addition to the two ports connected to the AC mains (P and N in Figure 2), each LISN has two ports: one for power connection (1 and 2 in Figure 2) and one for EMI measurements (3 and 4 in Figure 2). In order to accurately determine the relations between quantities at ports 1 and 2 and measurements performed at ports 3 and 4, it is possible to characterize the two LISNs as a four-port network, as depicted in Figure 5, yielding a 4 × 4 S-parameter matrix, denoted hereon as $\mathbf{S}_{LISN}$. The corresponding impedance matrix $\mathbf{Z}_{LISN}$ is obtained as follows:

$$\mathbf{Z}_{LISN} = Z_0(\mathbf{I}_4 + \mathbf{S}_{LISN})(\mathbf{I}_4 - \mathbf{S}_{LISN})^{-1} \tag{2}$$

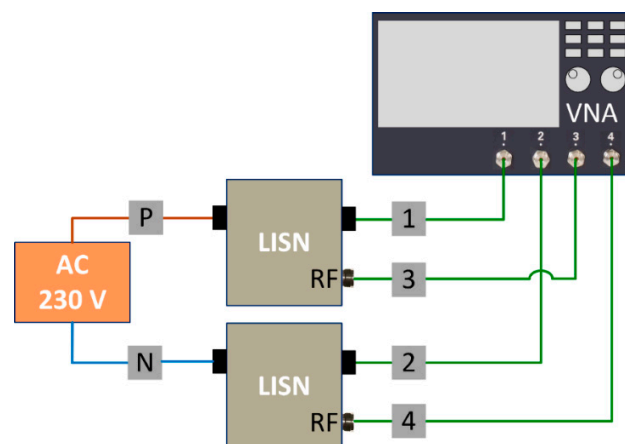where $\mathbf{I}_4$ is the 4 × 4 identity matrix.

Figure 5. Characterization of the two LISNs as a four-port network.

3.2. Characterization of Active Elements

The setup depicted in Figure 2 has been selected with the twofold purpose of determining a Thevenin model for the considered PLC systems and allowing the variation of LISN's impedances in order to verify the obtained model. In these regards, the corresponding circuit representation is depicted in Figure 6, where the PLC Tx is represented by its Thevenin equivalent circuit, while the PLC Rx and LISNs are represented by impedance matrices.
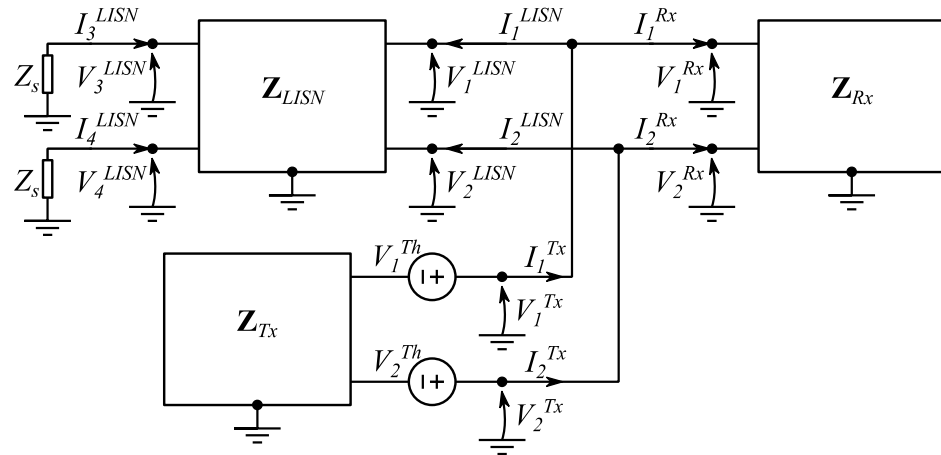

Figure 6. Calculation of the open-ended voltages of the Thevenin circuit in the PLC Tx model.

To evaluate open-ended voltage sources, V_1^{LISN} and V_2^{LISN}, the first step is to measure the voltages at the LISN's signal ports by means of an oscilloscope. The spectra of the time-domain measured voltages are then evaluated by the fast Fourier transform (FFT). The obtained frequency-domain voltages are hereinafter labeled as V_3^{LISN} and V_4^{LISN}. Therefore, neglecting the coaxial cable contributions, the currents drawn from the LISN signal ports I_3^{LISN} and I_4^{LISN} can be determined as follows:

$$I_3^{LISN} = -\frac{V_3^{LISN}}{Z_S} \tag{3}$$

$$I_4^{LISN} = -\frac{V_4^{LISN}}{Z_S} \tag{4}$$

where Z_S is the oscilloscope's input impedance.

Then, the voltages V_1^{LISN} and V_2^{LISN} and the currents I_1^{LISN} and I_2^{LISN} at the LISN's power ports can be determined by means of the ABCD representation of the LISN block, which is directly obtained from the measured S-parameters (see Section 3.1.2), as follows [25]:

$$\begin{bmatrix} V_1^{LISN} \\ V_2^{LISN} \\ I_1^{LISN} \\ I_2^{LISN} \end{bmatrix} = \begin{bmatrix} \mathbf{A}_{LISN} & \mathbf{B}_{LISN} \\ \mathbf{C}_{LISN} & \mathbf{D}_{LISN} \end{bmatrix} \begin{bmatrix} V_3^{LISN} \\ V_4^{LISN} \\ -I_3^{LISN} \\ -I_4^{LISN} \end{bmatrix} \tag{5}$$

Once voltages and currents at the LISN power ports are obtained from Equation (5), the circuit reported in Figure 6 can be solved to determine the voltage sources of the PLC Tx Thevenin equivalent circuit.

To this end, a two-port representation of all elements is required. Hence, the port constraints at the PLC Tx and PLC Rx and related transmission line ports are as follows:

$$\underbrace{\begin{bmatrix} V_1^{Rx} \\ V_2^{Rx} \end{bmatrix}}_{\mathbf{V}_{Rx}} = \mathbf{Z}_{Rx} \underbrace{\begin{bmatrix} I_1^{Rx} \\ I_2^{Rx} \end{bmatrix}}_{\mathbf{I}_{Rx}} \tag{6}$$

$$\underbrace{\begin{bmatrix} V_1^{Tx} \\ V_2^{Tx} \end{bmatrix}}_{\mathbf{V}_{Tx}} = \underbrace{\begin{bmatrix} V_1^{Th} \\ V_2^{Th} \end{bmatrix}}_{\mathbf{V}_{Th}} - \mathbf{Z}_{Tx} \underbrace{\begin{bmatrix} I_1^{Tx} \\ I_2^{Tx} \end{bmatrix}}_{\mathbf{I}_{Tx}} \tag{7}$$

where voltages and currents are defined as in Figure 6.

It is similarly needed to determine a 2×2 impedance representation of the LISNs. This requires converting the full 4×4 S-parameter matrix $\mathbf{S}_{LISN}$ into the corresponding 4×4 impedance matrix $\mathbf{Z}_{LISN}$, according to Equation (2). Successively, the desired 2×2 impedance matrix is obtained, considering that the LISN's signal ports are terminated on the oscilloscope port impedances Z_s, which are not necessarily equal to 50 Ω, as depicted in Figure 6. The port constraints at the LISN ports read:

$$\underbrace{\begin{bmatrix} V_1^{LISN} \\ V_2^{LISN} \\ V_3^{LISN} \\ V_4^{LISN} \end{bmatrix}}_{\mathbf{V}_{LISN}} = \mathbf{Z}_{LISN} \underbrace{\begin{bmatrix} I_1^{LISN} \\ I_2^{LISN} \\ I_3^{LISN} \\ I_4^{LISN} \end{bmatrix}}_{\mathbf{I}_{LISN}} \tag{8}$$

Substituting port constraints in Equations (3) and (4) into Equation (8), the equivalent 2×2 impedance matrix $\mathbf{Z}_{LISN}^{2 \times 2}$ seen from ports 1 and 2 of the LISNs is obtained as follows:

$$\underbrace{\begin{bmatrix} V_1^{LISN} \\ V_2^{LISN} \end{bmatrix}}_{\mathbf{V}_{LISN}^{2 \times 2}} = \underbrace{\begin{bmatrix} Z_{11}^{LISN} + k_{31} Z_{13}^{LISN} + k_{41} Z_{14}^{LISN} & Z_{12}^{LISN} + k_{32} Z_{13}^{LISN} + k_{42} Z_{14}^{LISN} \\ Z_{21}^{LISN} + k_{31} Z_{23}^{LISN} + k_{41} Z_{24}^{LISN} & Z_{22}^{LISN} + k_{32} Z_{23}^{LISN} + k_{42} Z_{24}^{LISN} \end{bmatrix}}_{\mathbf{Z}_{LISN}^{2 \times 2}} \underbrace{\begin{bmatrix} I_1^{LISN} \\ I_2^{LISN} \end{bmatrix}}_{\mathbf{I}_{LISN}^{2 \times 2}} \tag{9}$$

where

$$\begin{array}{ll} k_{31} = \frac{Z_{34}^{LISN} Z_{41}^{LISN} - Z_{31}^{LISN} \left(Z_{44}^{LISN} + Z_S \right)}{\left(Z_{33}^{LISN} + Z_S \right) \left(Z_{44}^{LISN} + Z_S \right) - Z_{34}^{LISN} Z_{43}^{LISN}}, & k_{32} = \frac{Z_{34}^{LISN} Z_{42}^{LISN} - Z_{32}^{LISN} \left(Z_{44}^{LISN} + Z_S \right)}{\left(Z_{33}^{LISN} + Z_S \right) \left(Z_{44}^{LISN} + Z_S \right) - Z_{34}^{LISN} Z_{43}^{LISN}} \\ k_{41} = \frac{Z_{43}^{LISN} Z_{31}^{LISN} - Z_{41}^{LISN} \left(Z_{33}^{LISN} + Z_S \right)}{\left(Z_{33}^{LISN} + Z_S \right) \left(Z_{44}^{LISN} + Z_S \right) - Z_{34}^{LISN} Z_{43}^{LISN}}, & k_{42} = \frac{Z_{43}^{LISN} Z_{32}^{LISN} - Z_{42}^{LISN} \left(Z_{33}^{LISN} + Z_S \right)}{\left(Z_{33}^{LISN} + Z_S \right) \left(Z_{44}^{LISN} + Z_S \right) - Z_{34}^{LISN} Z_{43}^{LISN}} \end{array} \tag{10}$$

and Z_{xy}^{LISN} indicates the (x,y) entry of matrix $\mathbf{Z}_{LISN}$.

Since the three two-port circuit elements are connected in parallel, i.e.,

$$\mathbf{V}_{LISN} = \mathbf{V}_{Rx} = \mathbf{V}_{Tx} \tag{11}$$

combining Equations (6), (7), (9) and (11), the equivalent voltage sources of the Thevenin equivalent circuit V_1^{Th} and V_2^{Th} are hence obtained as follows:

$$\mathbf{V}_{Th} = \left(\mathbf{Z}_{LISN}^{2 \times 2} + \mathbf{Z}_{Tx} + \mathbf{Z}_{Tx} \mathbf{Z}_{Rx}^{-1} \mathbf{Z}_{LISN}^{2 \times 2} \right) \mathbf{I}_{LISN} \tag{12}$$

4. Experimental Investigation

4.1. Test Setup

The experimental test setup is shown in Figure 7. The PLC Tx and Rx modems communicate through a short AC transmission line, which is connected to the 230 V AC mains through two HV-AN 150 LISNs. LISN measurement ports are connected to an oscilloscope (Keysight DSOX1204G) with the objective of measuring the noise from the system under test. The oscilloscope input impedance Z_S is set equal to 1 MΩ in parallel with a 16 pF capacitor [26]. This setup will be used both for the extraction of the active part of the model and for model validation, as LISNs offer proper ports for EMI measurement. The specific G3-PLC modems are Microchip ATMEL P360 with a maximum bandwidth of 500 kHz [27]. In this specific implementation, the two PLC modems communicate in

the CENELEC A band between 35 and 91 kHz; in this frequency range, the PLC Tx can be regarded as an intentional noise source. Five thousand frames of data are sent from the transmitter modem to the PLC receiver with a 100 ms lag between consecutive frames. The PHY layer specifications of the G3-PLC modem (see details in [28]) are summarized in Table 1.
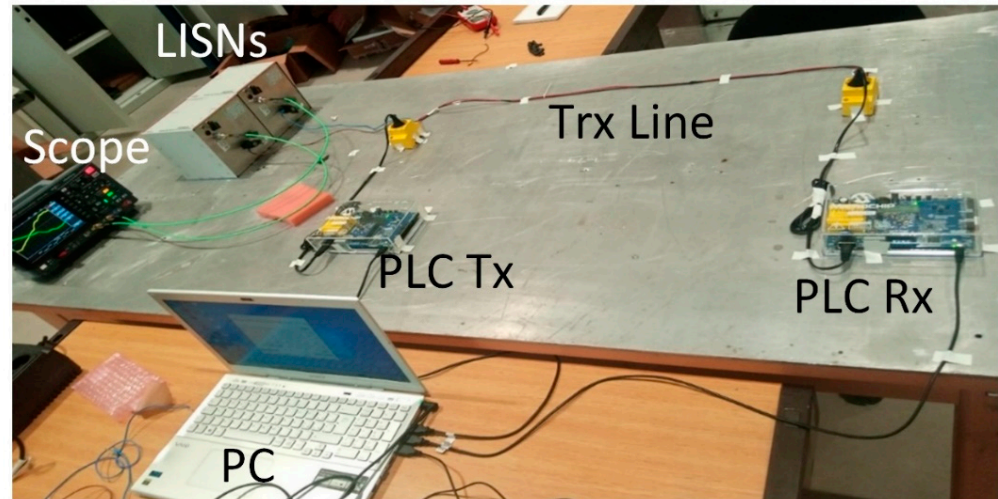

Figure 7. Experimental test bench to measure the active part of the model.

Table 1. PHY layer specifications of the G3-PLC modems considered in this work.

Feature	Parameter
Modulation	OFDM
No. of sub-carriers	36
Frequency band	CENELEC A (35 kHz–91 kHz)
Sub-carrier modulation	BPSK
Max data rate	up to 34 kbps
Sent frames	5000
Time between frames	50 ms

The operating mode of the HV-AN 150 LISN can be switched to comply with several EMC standards, including the most common CISPR 16-1-2, CISPR 25, MIL-STD 461F, and DOG-160G standards [29]. Therefore, they can be easily exploited to generate different working conditions. To extract the active part of the behavioral model, the LISNs are configured to work for DOG-160G (LISN A). This will be referred to as the "reference case" hereafter. Then, the following two cases are considered for model validation. In the former test case (case #1), the DOG-160G standard LISNs are modified by adding 0.047 µF capacitors at the EUT sides (LISN B1). The second test case (case #2) is obtained by adding the same 0.047 µF capacitors at the EUT sides of the CISPR 25 LISNs (LISN B2). The aforementioned test cases are gathered in Table 2 and shown in Figure 8.

Table 2. LISN setups used to realize different working conditions.

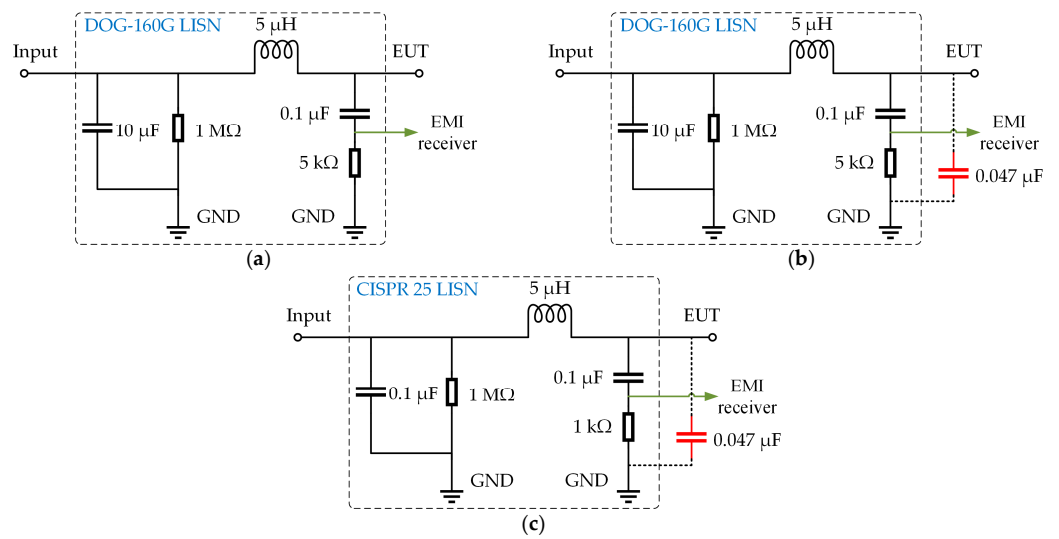| Case	Implementation
Reference (LISN A)	DOG-160G
#1 (LISN B1)	DOG-160G + 0.047 uF capacitors at the EUT sides
#2 (LISN B2)	CISPR 25 + 0.047 uF capacitors at the EUT sides

Figure 8. (**a**) DOG-160G LISN (LISN A), (**b**) LISN B1, and (**c**) LISN B2 used for model extraction (**a**) and verification (**b**,**c**). Only one line (P or N with ground) is shown.

Figure 9 shows the test setup to characterize the LISNs. The LISNs are characterized in the frequency domain by a four-port VNA (Keysight E5080B ENA). The measured input impedances of the LISNs seen from ports 1 and 2 are plotted in Figure 10. The comparison proves that the LISNs show different impedances, and therefore it is possible to use LISN B1 and LISN B2 to generate different working conditions.
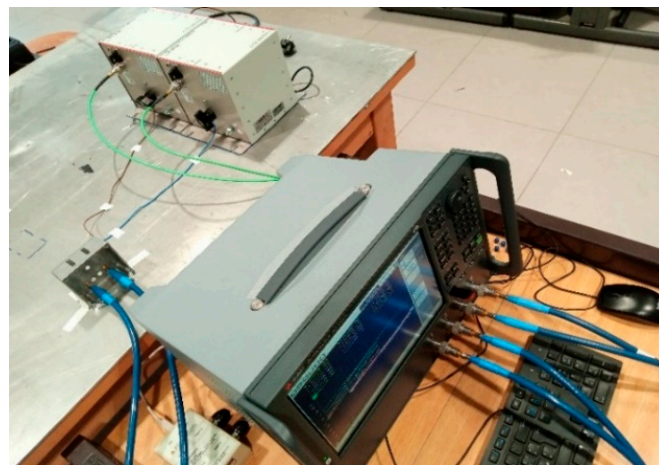
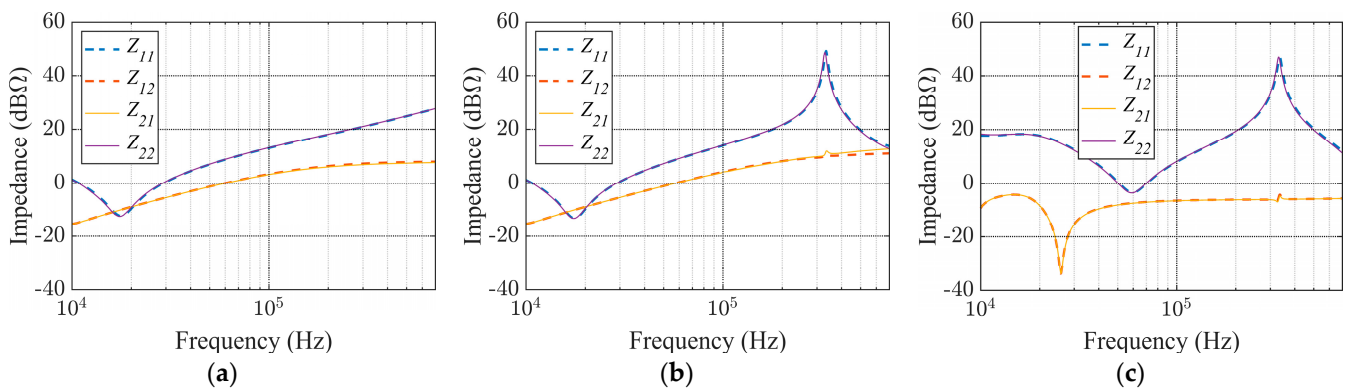**Figure 9.** Experimental test bench to characterize the LISNs.

Figure 10. Impedance plots: (**a**) DOG-160G LISN (LISN A), (**b**) LISN B1, and (**c**) LISN B2.

4.2. Extraction of the Behavioral Model

Figure 11 shows the experimental test setups used to characterize the PLC modems: The Tx modem is characterized separately (left panel), whereas the Rx modem is characterized together with the transmission line and the load (right panel). The measured impedances are shown in Figure 12a,b.
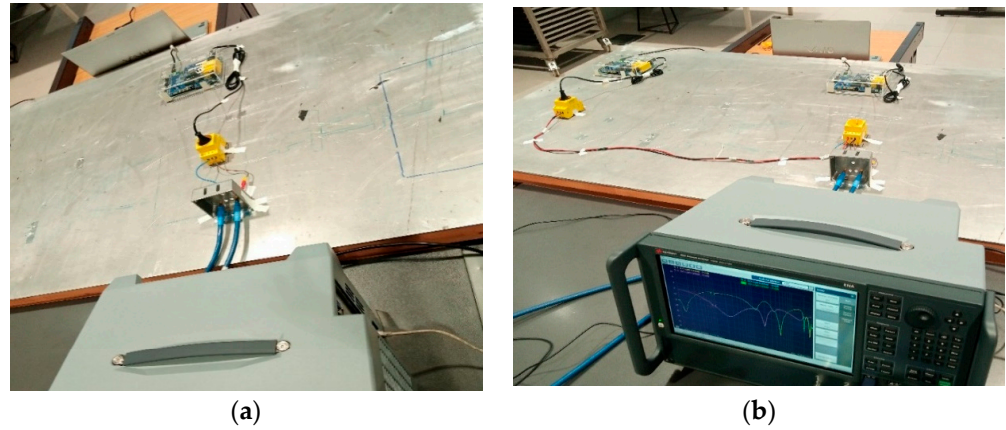

(a)   (b)

Figure 11. Experimental test bench to characterize (**a**) the PLC Tx modem and (**b**) the PLC Rx modem together with the transmission line.
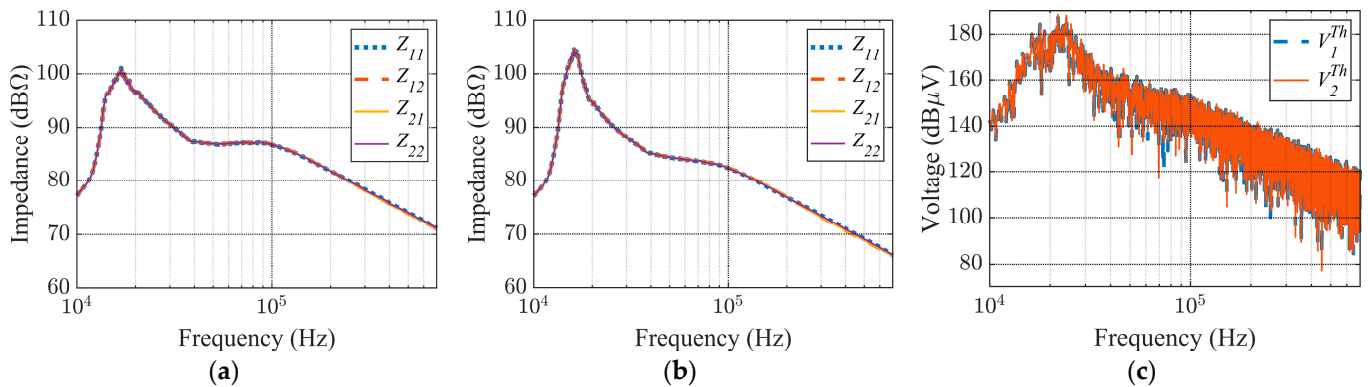

Figure 12. Behavioral model parameters: impedances of (**a**) the PLC Tx modem and (**b**) the PLC Rx modem together with the transmission line; and (**c**) equivalent voltage sources.

To extract the active part of the behavioral model, measurement is carried out with the setup shown in Figure 7, where reference LISN (LISN A) is exploited. Then, the equivalent voltage sources $\mathbf{V}_{Th-A} = \left[V_1^{Th}; V_2^{Th} \right]$ can be obtained by Equation (12) and plotted (Figure 12c).

4.3. Results and Discussions

To verify the accuracy of the extracted behavioral model, the other two LISNs are employed in place of LISN A in Figure 7. More specifically, cases #1 and #2 involve LISNs B1 and B2, respectively. As shown in Figure 10, their impedances significantly differ from LISN A, thus ensuring sufficiently different working conditions ($\mathbf{Z}_{LISN-B1,B2}^{2\times2}$). Predictions of line currents are obtained by exploiting the behavioral model as follows:

$$\mathbf{I}_{LISN-B1,B2} = \left(\mathbf{Z}_{LISN-B1,B2}^{2\times2} + \mathbf{Z}_{Tx} + \mathbf{Z}_{Tx}\mathbf{Z}_{Rx}^{-1}\mathbf{Z}_{LISN-B1,B2}^{2\times2} \right)^{-1} \mathbf{V}_{Th-A} \qquad (13)$$

Figure 13 shows the line currents obtained from the prediction and measurement of test case #1. The measured and predicted currents show good consistency below 100 kHz, while some discrepancies are present above 100 kHz. This might be due to the fact that

the characteristics of the reference LISN A and the verification LISN (in this case, LISN B1) have the same impedance below 100 kHz, while their impedance is different at higher frequencies. This can be noticed by comparing Figure 8a,b. Therefore, to estimate the accuracy of the model below 100 kHz, test case #2 is considered. The results are presented in Figure 14, which shows that the behavioral model cannot accurately predict the emissions below 100 kHz when the working condition changes. These results indicate that the model introduced in Section 3 cannot accurately reproduce the behavior of the PLC Tx modem since the assumption of linearity is not satisfied due to the presence of the embedded control systems. Indeed, PLC modems are designed to inject a controlled signal into the grid, and the output voltage is related to the output current through suitable control loops.
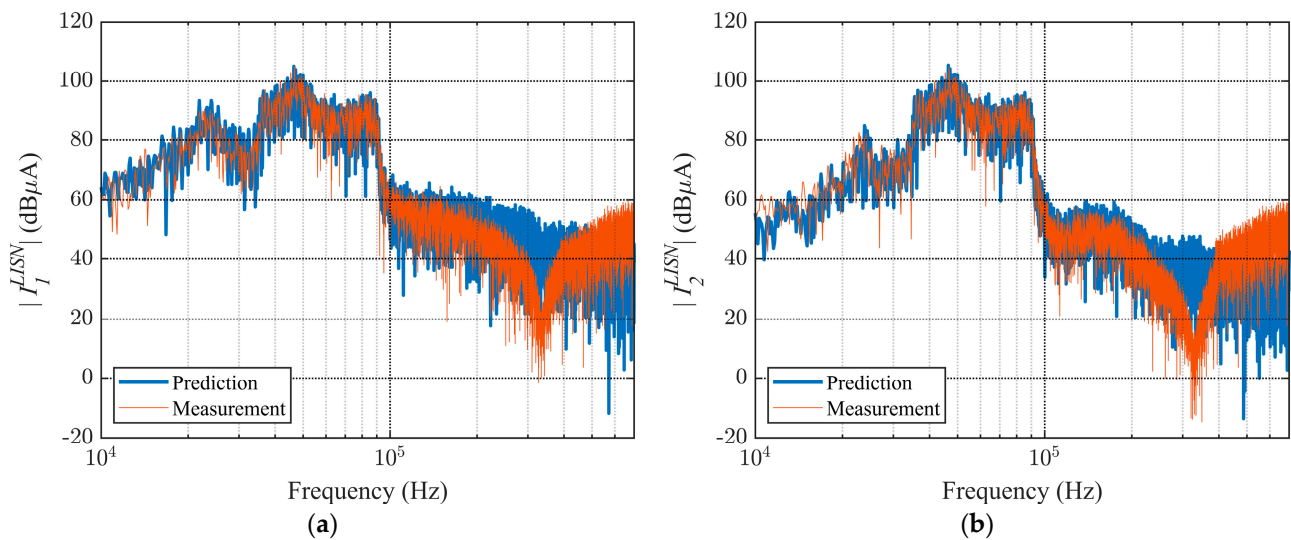

Figure 13. Currents (**a**) I_1^{LISN} and (**b**) I_2^{LISN} obtained from the prediction model and measurement data in test case #1 (with LISN B1). The PLC Tx modem is represented according to Section 3.
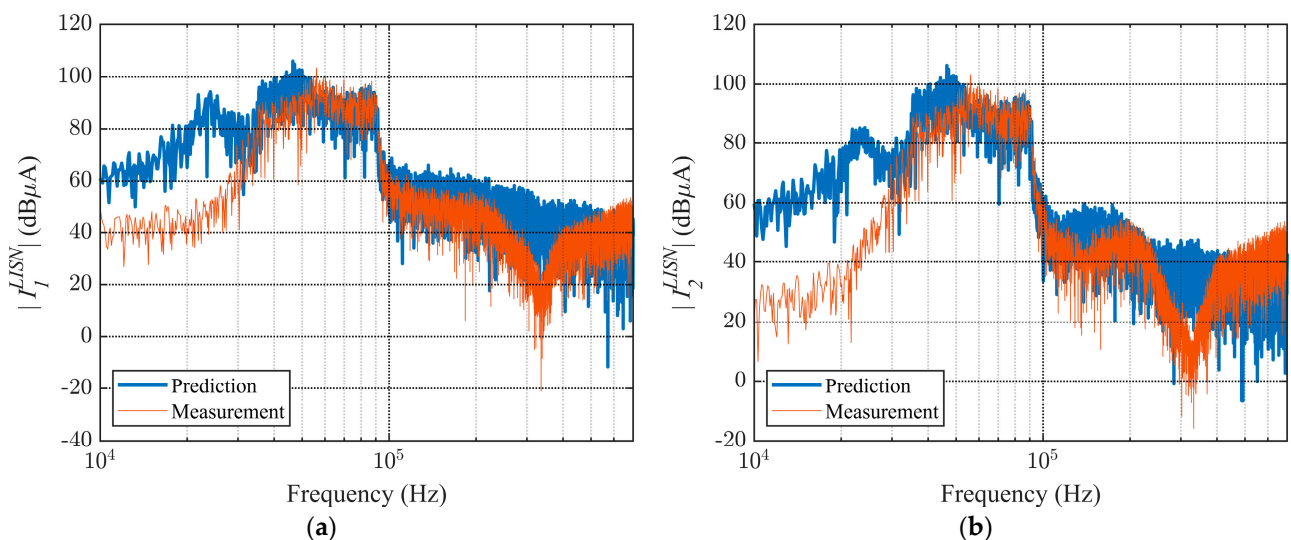

Figure 14. Currents (**a**) I_1^{LISN} and (**b**) I_2^{LISN} obtained from the prediction model and the measurement of test case #2 (with LISN B2). The PLC Tx modem is represented according to Section 3.

5. Alternative Behavioral Model of PLC Tx

5.1. Modeling Procedure

To overcome the previously outlined limitation and provide effective modeling of the PLC Tx modem, an alternative approach based on the substitution theorem is proposed. Specifically, since the closed-loop control keeps the voltage level at the modem output

constant, the idea is to substitute the PLC Tx modem with a pair of ideal voltage sources. This model should therefore be valid at least in the frequency range in which the internal control algorithms work properly and in a reasonable range of system impedances. The PLC Rx and LISN models are unchanged.

Accordingly, the circuit in Figure 6 is revised as reported in Figure 15. Since the PLC Tx is modelled as a pair of ideal voltage sources, the voltages at the LISN's power ports are equal to the PLC Tx equivalent voltage sources. As a consequence, the voltage sources are obtained directly from the voltages measured in the LISN-A setup, as:

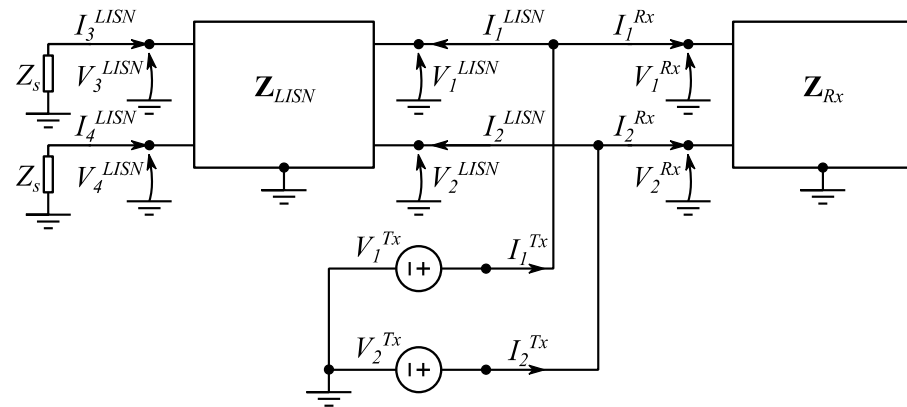$$\mathbf{V}_{Tx} = \mathbf{V}_{LISN-A}^{2\times2} \tag{14}$$

Figure 15. Calculation of PLC Tx equivalent voltage sources.

The frequency response of the voltage sources in Equation (14) is plotted in Figure 16.
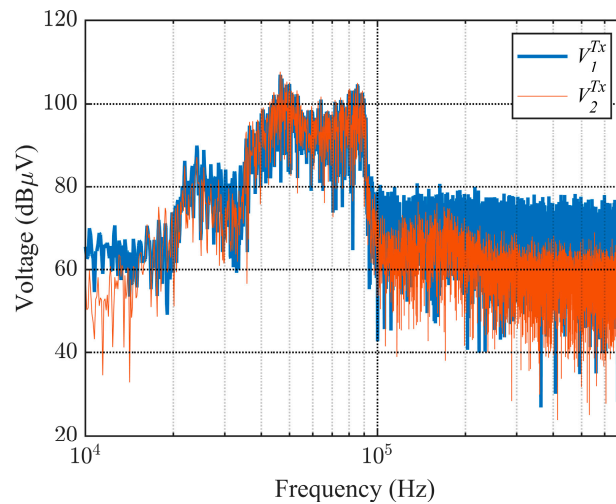

Figure 16. Equivalent voltage sources used to represent the PLC Tx modem.

5.2. Experimental Validation

Model validation is achieved by comparing the currents predicted by the model, i.e.,

$$\mathbf{I}_{LISN-B} = \mathbf{Z}_{LISN-B}^{2\times2}{}^{-1}\mathbf{V}_{Tx} \tag{15}$$

with the same currents obtained from the measurements in the LISN-B setups. Concerning test case #1, the predicted currents based on the proposed model are compared with the measurement results in Figure 17. The comparison reveals an appreciable improvement in line current prediction up to 500 kHz, which is the maximum frequency of the NB G3-PLC. As explained in Section 4.2, since the measured currents with LISN A and LISN B1 are the

same below 100 kHz, an additional test (case #2) with LISN B2 is required to assess the low-frequency behavior. The results are shown in Figure 18. Measured and predicted line currents show good agreement up to 500 kHz, including the range below 100 kHz. These results confirm that, even though some differences between measurements and predictions are still present, the proposed PLC Tx modem model outperforms the model in Section 3.2 (see Figure 15 for reference). This improvement can also be quantified by considering standard error indicators, such as the mean absolute error (MAE) presented in Table 3. Indeed, G3-PLC modems provide a spectrum with constant amplitude in the frequency range between 35 and 91 kHz according to the standard ITU-T G. 9901. Additionally, the control system inside them and the robust modulation schemes (OFDM) in this PLC protocol allow a constant spectrum up to 500 kHz. At higher frequencies, the effect of the PLC control system will progressively fade, resulting in an LTI system, as it happens for power converters [30] at frequencies sufficiently higher than those at which the converter control system operates.
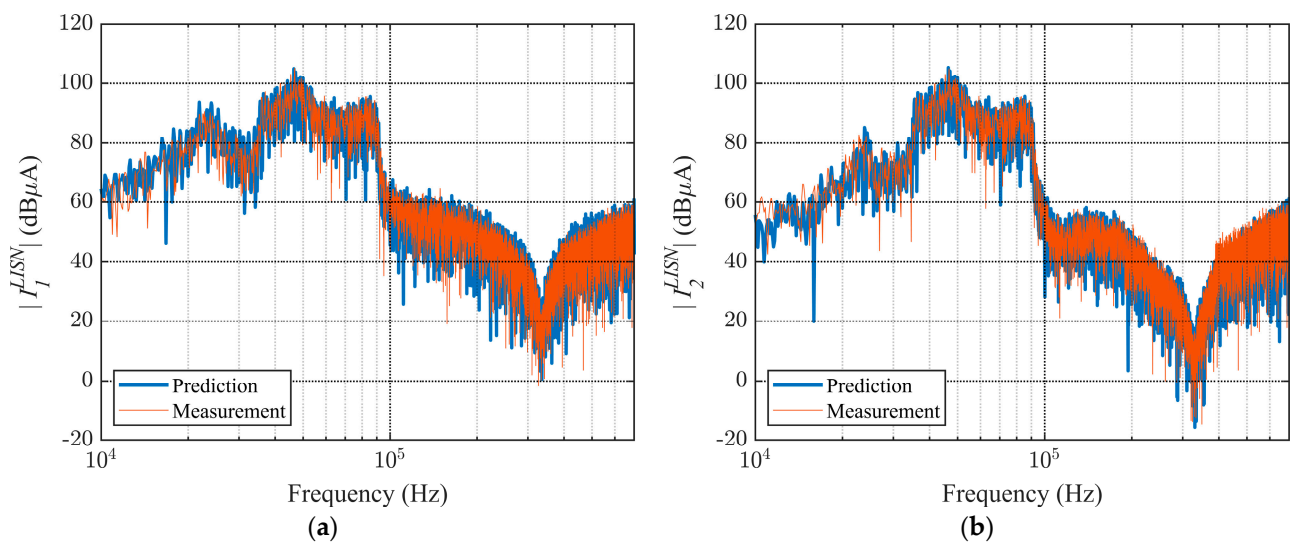

Figure 17. Currents (**a**) I_1^{LISN} and (**b**) I_2^{LISN} obtained from the prediction model and measurement data in test case #1 (with LISN B1). The PLC Tx modem is represented according to Section 5.

Figure 18. Currents (**a**) I_1^{LISN} and (**b**) I_2^{LISN} obtained from the prediction model and measurement data in test case #2 (with LISN B2). The PLC Tx modem is represented according to Section 5.
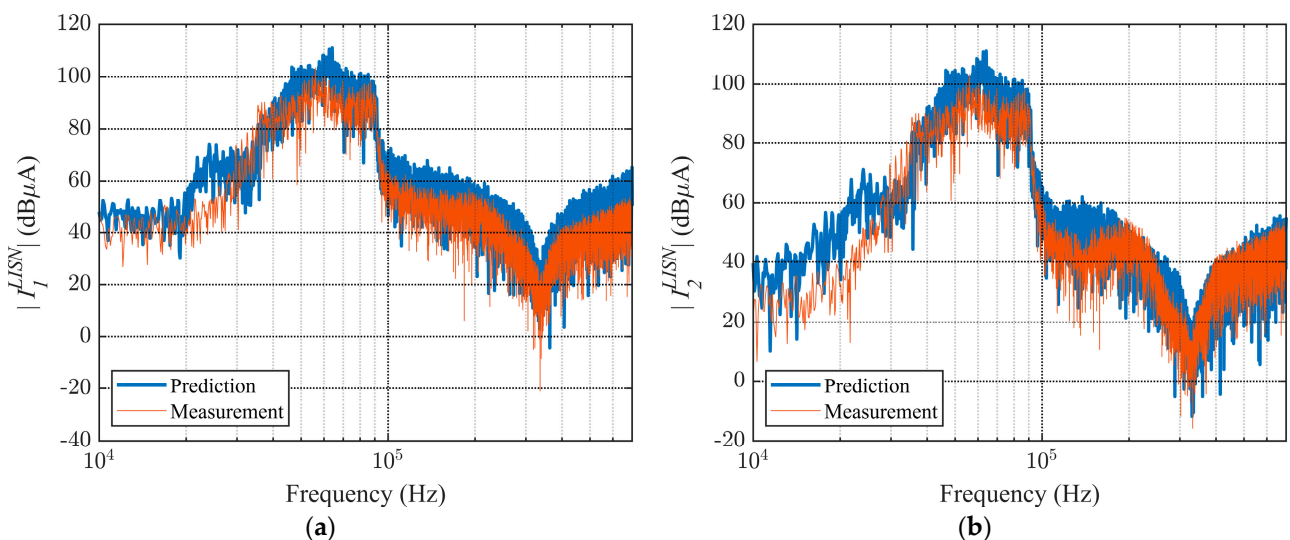
Table 3. MAEs of the current curves shown in Figures 13, 14, 17 and 18.

Test Case	Current	Model in Section 3.2	Model in Section 5.1
#1	I_1^{LISN}	25.32	12.60
	I_2^{LISN}	26.52	14.60
#2	I_1^{LISN}	20.94	11.21
	I_2^{LISN}	21.81	14.57

6. Conclusions

In this work, an experimental investigation aimed at developing behavioral models for G3-PLC modems suitable for EMI analysis in complex power networks is presented. Different modeling strategies for the PLC Tx and Rx modems were proposed to account for the different behaviors of the modems in transmitting and receiving mode. Equivalent representations of the modems in terms of Thevenin equivalent circuits were investigated as the first step. However, experimental results proved that a linear representation of the G3-PLC modem, although effective when the modem is in receiving mode, is not feasible for the transmitting modem, due to the modem internal control system.

Hence, an alternative representation of the PLC Tx modem is proposed, which resorts to a pair of ideal voltage sources in accordance with the substitution theorem. This modeling approach was proven to accurately represent G3-PLC modems in the frequency band of interest and is in line with the ITU-T G. 9901 Standard, which specifies the amplitude of the spectrum in which G3-PLC modems ensure constant amplitude in the frequency interval of interest (below 500 kHz). In future work, the proposed models of PLC modems will be used to investigate the coexistence between communication systems and high-power switching devices in complex power networks.

Author Contributions: Conceptualization, A.H.B., S.N. and F.G., methodology, A.H.B., S.N., L.W., F.G., G.S. and X.W.; validation, A.H.B., S.N., X.W., X.L., L.W., F.G. and G.S.; formal analysis, A.H.B., S.N. and F.G.; investigation, A.H.B., G.S. and F.G.; resources, F.G., G.S. and S.A.P.; data curation, A.H.B., S.N. and X.W.; writing—original draft preparation, A.H.B. and F.G.; writing—review and editing, A.H.B., S.N., F.G., G.S., X.W., X.L., L.W. and S.A.P.; visualization, F.G. and G.S.; supervision, F.G. and G.S.; project administration, F.G.; funding acquisition, F.G. All authors have read and agreed to the published version of the manuscript.

Data Availability Statement: Not applicable.

Conflicts of Interest: The authors declare no conflict of interest.

References

1. Impram, S.; Nese, S.V.; Oral, B. Challenges of renewable energy penetration on power system flexibility: A survey. *Energy Strategy Rev.* **2020**, *31*, 100539. [CrossRef]
2. Moreno Escobar, J.J.; Morales Matamoros, O.; Tejeida Padilla, R.; Lina Reyes, I.; Quintana Espinosa, H. A Comprehensive Review on Smart Grids: Challenges and Opportunities. *Sensors* **2021**, *21*, 6978. [CrossRef] [PubMed]
3. Ancillotti, E.; Bruno, R.; Conti, M. The role of communication systems in smart grids: Architectures, technical solutions and research challenges. *Comput. Commun.* **2013**, *36*, 1665–1697. [CrossRef]
4. Kabalci, Y. A survey on smart metering and smart grid communication. *Renew. Sustain. Energy Rev.* **2016**, *57*, 302–318. [CrossRef]
5. Uribe-Pérez, N.; Angulo, I.; De la Vega, D.; Arzuaga, T.; Fernández, I.; Arrinda, A. Smart Grid Applications for a Practical Implementation of IP over Narrowband Power Line Communications. *Energies* **2017**, *10*, 1782. [CrossRef]
6. Sendin, A.; Simon, J.; Urrutia, I.; Berganza, I. PLC deployment and architecture for Smart Grid applications in Iberdrola. In Proceedings of the 18th IEEE International Symposium on Power Line Communications and Its Applications, Glasgow, UK, 30 March–2 April 2014; pp. 173–178.
7. Khan, M.S.; Ahmed, T.; Aziz, I.; Alam, F.B.; Bhuiya, M.S.U.; Alam, M.J.; Chakma, R.; Mahtab, S.S. PLC Based Energy-Efficient Home Automation System with Smart Task Scheduling. In Proceedings of the 2019 IEEE Sustainable Power and Energy Conference (ISPEC), Beijing, China, 21–23 November 2019; pp. 35–38.

8. Lopez, G.; Matanza, J.; De La Vega, D.; Castro, M.; Arrinda, A.; Moreno, J.I.; Sendin, A. The role of power line communications in the smart grid revisited: Applications challenges and research initiatives. *IEEE Access* **2019**, *7*, 117346–117368. [CrossRef]
9. Beshir, A.H.; El Sayed, W.; Wan, L.; Grassi, F.; Crovetti, P.S.; Liu, X.; Wu, X.; Madi, A.; Smolenski, R.; Pignari, S.A. Influence of Random Modulated Power Converter on G3 Power Line Communication. *Appl. Sci.* **2022**, *12*, 5550. [CrossRef]
10. Kharanaq, F.A.; Emadi, A.; Bilgin, B. Modelling of Conducted Emissions for EMI Analysis of Power Converters: State-of-the-Art Review. *IEEE Access* **2020**, *8*, 189313–189325. [CrossRef]
11. Riba, J.-R.; Moreno-Eguilaz, M.; Bogarra, S.; Garcia, A. Parameter Identification of DC-DC Converters under Steady-State and Transient Conditions Based on White-Box Models. *Electronics* **2018**, *7*, 393. [CrossRef]
12. Negri, S.; Wu, X.; Liu, X.; Grassi, F.; Spadacini, G.; Pignari, S.A. Mode Conversion in DC-DC Converters with Unbalanced Busbars. In Proceedings of the 2019 Joint International Symposium on Electromagnetic Compatibility, Sapporo and Asia-Pacific International Symposium on Electromagnetic Compatibility (EMC Sapporo/APEMC), Sapporo, Japan, 3–7 June 2019; pp. 112–115.
13. Spadacini, G.; Grassi, F.; Bellan, D.; Pignari, S.A.; Marliani, F. Prediction of Conducted Emissions in Satellite Power Buses. *Int. J. Aerosp. Eng.* **2015**, *2015*, 601426. [CrossRef]
14. Baisden, A.C.; Boroyevich, D.; Wang, F. Generalized Terminal Modeling of Electromagnetic Interference. *IEEE Trans. Ind. Appl.* **2010**, *46*, 2068–2079. [CrossRef]
15. Wan, L.; Beshir, A.H.; Wu, X.; Liu, X.; Grassi, F.; Spadacini, G.; Pignari, S.A.; Zanoni, M.; Tenti, L.; Chiumeo, R. Black-Box Modelling of Low-Switching-Frequency Power Inverters for EMC Analyses in Renewable Power Systems. *Energies* **2021**, *14*, 3413. [CrossRef]
16. Donnelly, T.J.; Pekarek, S.D.; Fudge, D.R.; Zarate, N. Thévenin Equivalent Circuits for Modeling Common-Mode Behavior in Power Electronic Systems. *IEEE Open Access J. Power Energy* **2020**, *7*, 163–172. [CrossRef]
17. Amara, M.; Vollaire, C.; Ali, M.; Costa, F. Black Box EMC Modelling of a Three Phase Inverter. In Proceedings of the 2018 International Symposium on Electromagnetic Compatibility (EMC EUROPE), Amsterdam, The Netherlands, 27–30 August 2018; pp. 642–647.
18. Kabalci, E.; Kabalci, Y.; Develi, I. Modelling and analysis of a power line communication system with QPSK modem for renewable smart grids. *Int. J. Electr. Power Energy Syst.* **2012**, *34*, 19–28. [CrossRef]
19. Beshir, A.H.; Wan, L.; Grassi, F.; Crovetti, P.S.; Liu, X.; Wu, X.; El Sayed, W.; Spadacini, G.; Pignari, S.A. Electromagnetic Interference of Power Converter with Random Modulation on the Power Line Communication System. *Electronics* **2021**, *10*, 2979. [CrossRef]
20. Del Puerto-Flores, J.A.; Naredo, J.L.; Peña-Campos, F.; Del-Valle-Soto, C.; Valdivia, L.J.; Parra-Michel, R. Channel Characterization and SC-FDM Modulation for PLC in High-Voltage Power Lines. *Future Internet* **2022**, *14*, 139. [CrossRef]
21. Barmada, S.; Raugi, M.; Tucci, M.; Maryanka, Y.; Amrani, O. PLC systems for electric vehicles and Smart Grid applications. In Proceedings of the 2013 IEEE 17th International Symposium on Power Line Communications and Its Applications, Johannesburg, South Africa, 24–27 March 2013; pp. 23–28.
22. Kami, Y.; Xiao, F.; Murano, K. Mode-port-network approach to analyze power-line EMC problems for PLC. In Proceedings of the 20th International Zurich Symposium on Electromagnetic Compatibility, Zurich, Switzerland, 12–16 January 2009; pp. 9–12.
23. Grassi, F.; Wu, X.; Yang, Y.; Spadacini, G.; Pignari, S.A. Modeling of imbalance in differential lines targeted to SPICE simulation. *Prog. Electromagn. Res. B* **2015**, *62*, 225–239. [CrossRef]
24. Sayed, W.E.; Lezynski, P.; Smolenski, R.; Madi, A.; Pazera, M.; Kempski, A. Deterministic vs. Random Modulated Interference on G3 Power Line Communication. *Energies* **2021**, *14*, 3257. [CrossRef]
25. Reveyrand, T. Multiport conversions between S, Z, Y, h, ABCD, and T parameters. In Proceedings of the 2018 International Workshop on Integrated Nonlinear Microwave and Millimetre-wave Circuits (INMMIC), Brive La Gaillarde, France, 5–6 July 2018; pp. 1–3.
26. DSOX1204G Oscilloscope Datasheet. Available online: https://www.keysight.com/us/en/product/DSOX1204G/oscilloscope-70-100-200-mhz-4-analog-channels-waveform-generator.html (accessed on 1 March 2023).
27. PL360-EK Quick Start User Guide. Available online: https://ww1.microchip.com/downloads/en/DeviceDoc/PL360-EK-Quick-Start-User-Guide-DS50002752A.pdf (accessed on 1 March 2023).
28. PL360-EK User Guide. Available online: https://www.microchip.com/en-us/product/PL360B (accessed on 1 March 2023).
29. LISN Manual. Available online: .https://www.ametek-cts.com/products/brands/teseq/hv-an-150 (accessed on 1 March 2023).
30. Wan, L.; Beshir, A.H.; Wu, X.; Liu, X.; Grassi, F.; Spadacini, G.; Pignari, S.A. Black-box Modeling of Converters in Renewable Energy Systems for EMC Assessment: Overview and Discussion of Available Models. *Chin. J. Electr. Eng.* **2022**, *8*, 13–28. [CrossRef]